Metals and Materials International (2018) 24:773–788
https://doi.org/10.1007/s12540-018-0084-9

Contributions of Rare Earth Element (La,Ce) Addition to the Impact Toughness of Low Carbon Cast Niobium Microalloyed Steels

Hadi Torkamani[1] · Shahram Raygan[1] · Carlos Garcia Mateo[2] · Jafar Rassizadehghani[1] · Yahya Palizdar[3] · David San-Martin[2]

Received: 4 September 2017 / Accepted: 20 December 2017 / Published online: 13 March 2018

Abstract
In this research Rare Earth elements (RE), La and Ce (200 ppm), were added to a low carbon cast microalloyed steel to disclose their influence on the microstructure and impact toughness. It is suggested that RE are able to change the interaction between the inclusions and matrix during the solidification process (comprising peritectic transformation), which could affect the microstructural features and consequently the impact property; compared to the base steel a clear evolution was observed in nature and morphology of the inclusions present in the RE-added steel i.e. (1) they changed from MnS-based to (RE,Al)(S,O) and RE(S)-based; (2) they obtained an aspect ratio closer to 1 with a lower area fraction as well as a smaller average size. Besides, the microstructural examination of the matrix phases showed that a bimodal type of ferrite grain size distribution exists in both base and RE-added steels, while the mean ferrite grain size was reduced from 12 to 7 μm and the bimodality was redressed in the RE-added steel. It was found that pearlite nodule size decreases from 9 to 6 μm in the RE-added steel; however, microalloying with RE caused only a slight decrease in pearlite volume fraction. After detailed fractography analyses, it was found that, compared to the based steel, the significant enhancement of the impact toughness in RE-added steel (from 63 to 100 J) can be mainly attributed to the differences observed in the nature of the inclusions, the ferrite grain size distribution, and the pearlite nodule size. The presence of carbides (cementite) at ferrite grain boundaries and probable change in distribution of Nb-nanoprecipitation (promoted by RE addition) can be considered as other reasons affecting the impact toughness of steels under investigation.

Keywords RE addition · Cast microalloyed steel · Impact toughness · Grain size · Inclusion

1 Introduction

Although wrought grades of microalloyed steels have been available for decades, producing low-cost high strength cast steels is still highly demanded. The carbon content of these steels can be reduced to improve both weldability and toughness resulting in strength reductions, which can be compensated by microalloying additions [1–4]. So far, low carbon cast microalloyed steels have found many applications in the production of complex internal shapes and the manufacturing of industrial parts where a high impact toughness at room temperature is desired [1, 5].

Generally, the solidification path followed by these low carbon microalloyed steels comprises a peritectic reaction/transformation. Although this transformation is regarded as an important source of crack-formation [6–8], it has been studied with less detail compared to other widespread transformations in steels. According to John and Hogan [9] this transformation

✉ Hadi Torkamani
H.torkamani@ut.ac.ir

✉ Shahram Raygan
Shraygan@ut.ac.ir

✉ Carlos Garcia Mateo
cgm@cenim.csic.es

[1] School of Metallurgy and Materials Engineering, College of Engineering, University of Tehran, P.O. Box 11155-4563, Tehran, Iran

[2] Materalia Research Group, National Center for Metallurgical Research (CENIM), Consejo Superior de Investigaciones Cientificas (CSIC), Avda Gregorio del Amo, 8, E-28040 Madrid, Spain

[3] Materials and Energy Research Center, Karaj 3177983634, Iran

can be described as two consecutive steps: (1) the "peritectic reaction" and (2) the "peritectic transformation". In the current context, the "peritectic reaction" would refer to the step in which the new peritectic phase is in formation and three phases exist in conjunction with each other (triple point). During the peritectic reaction, austenite nucleates at the interface between the melt (L) and δ-ferrite [8, 10–13] and grows on the surface of the δ-ferrite forming a thin (1–5 μm) interrupting enclosure/layer around this phase [12, 14]. The "peritectic transformation" describes what follows after the peritectic reaction has taken place; i.e. the δ-phase is surrounded completely by a rim/layer of austenite and no triple points exist. In this second stage, the advance of the reaction is controlled by volume diffusion from the melt through the layer of the γ-phase towards the δ-phase direction. In this process, the layer of γ-phase thickens by its simultaneous growth into the melt and into the δ-phase until the transformation of δ-ferrite is completed [15]. The amount of γ that is the product of δ-ferrite to γ transformation may cause the generation of residual tensile stresses in the solidified steels due to the difference in density and packing factor between δ-ferrite and γ [11, 16, 17]. The distribution and size of this transformed austenite can affect how other phases transform upon cooling to room temperature, how the residual stress redistribute and, consequently, the steels toughness.

In the as-cast ferritic-pearlitic microstructure of low carbon steels, pearlite is a detrimental constituent to the impact toughness [18, 19]. The contribution of this phase to the Fracture Appearance Transition Temperature (FATT) has been expressed by the following equation [20]:

$$\Delta\mathrm{FATTp}\,(^{\circ}\mathrm{C}) = 15\left(V_P\right)^{\frac{1}{3}} \tag{1}$$

Apart from the amount of pearlite (V_P in vol%), in fully pearlitic steels, the mechanical properties are influenced by the pearlite microstructure such as nodule and colony size and also the thickness and interlamellar spacing of cementite [19, 21, 22]. However, in steels with a ferritic matrix, the influence of pearlite parameters like the nodule size and its volume fraction on the mechanical properties is more striking than other features [23]. Besides, it is well established that finer ferrite grains would enhance the impact toughness of steels [24–26].

Grain Boundary Carbides (GBC) are also considered as crack initiators that may impair the impact toughness [20, 24, 26]. The contribution of these carbides to the FATT depends on their thickness (t, in μm) and has been formulated as follows [26]:

$$\Delta\mathrm{FATTc}\,(^{\circ}\mathrm{C}) = 112\mathrm{t}^{\frac{1}{2}} \tag{2}$$

Mintz et al. [20] suggested that the linear relationship between the FATT and the square root of t, is more applicable in the range of average carbide thicknesses of 0.2–0.8 μm. Above and below these values, the influence of the carbide thickness on the transition temperature can be discarded. Gutiérrez [26, 27] has done deep studies on the effects of microstructure on the impact toughness of low carbon microalloyed steels. She suggested that for low carbon ferritic–pearlitic steels, the FATT would be related to the steel composition and to a series of microstructural contributions, proposing the following equation:

$$\begin{aligned}\mathrm{FATT}(^{\circ}\mathrm{C}) = &-1\mathrm{Mn} + 42\mathrm{Si} + 700(\mathrm{Nfree})^{\frac{1}{2}} \\ &+ 15\left(V_P\right)^{\frac{1}{3}} + 112\mathrm{t}^{\frac{1}{2}} + 0.5\Delta\sigma\mathrm{y} - 14(\mathrm{D})^{-\frac{1}{2}}\end{aligned} \tag{3}$$

where Nfree refers to the solute Nitrogen content, t is the thickness of GBC (in μm); D is the effective cleavage unit size in μm (for ferrite, D is usually taken as the mean grain size) and V_P is the amount of pearlite in vol%. This equation shows that the FATT is also a function of the strengthening term Δσy (accounting for all the eventual microstructural hardening contributions to the yield strength such as precipitation hardening but excluded from those resulting from the grain size).

In steelmaking industry, RE metals are known as strong sulfide, oxide, or oxysufide formers. The RE-based inclusions are formed in the molten steel providing the prospective heterogonous nuclei for other phases during the solidification of the steel [28–30]. The main function of RE in steel industry up to date has been orientated towards their ability to control the inclusions shape and keep them spherical through the hot deformation processes [31–34]. Furthermore, it has been stated that RE-particles are able to slow down the austenite grain growth at high temperature by Zener pinning [35–39].

In this work authors have investigated the other aspects of addition of Rare Earth (RE) elements such as La and Ce to low carbon cast microalloyed steels. To the author's knowledge, Gulyayev and Ulyanin [40] made the earliest reference to the effect of RE in steels in 1961. They discovered that unlike B, minor addition of RE can increase the toughness and reduce the sensibility to temper brittleness. In 1965, Belyakova et al. [41] asserted that the addition of RE into the ingot greatly increases the impact toughness by a factor of about 1.5 which has been mainly attributed to the inclusions characteristics. Since then, abundant investigations have focused on the effects of RE on the toughness property [42–48], most of which regard with wrought steels. These studies have reported different contributions of RE additions to the steel properties, although some of the results are somehow contradictory. Other reports evidenced that: (1) RE atoms may segregate to grain boundaries, lowering their energy, and making it difficult for other impurities to segregate and form compounds at these locations [31, 32]; (2) the impurities would combine with RE forming stable particles; as a result, cleaner grain boundaries would be obtained, improving the toughness [41]; (3) RE can enhance

Table 1 Chemical composition of the base steel (Fe to balance)

Elements	C	Si	Mn	S	P	V	Nb	Mo	Cu	Al	Cr
wt. %	0.16	0.30	1.00	0.01	0.02	0.11	0.05	0.01	0.09	0.04	0.06

the solubility of Nb in steels [44, 49] which would indirectly assist the nanoprecipitation of Nb(C,N) in microalloyed steels [50]. These precipitates are able to prevent the grain growth (at high temperatures) as well as to hinder dislocation movement during deformation, impeding the failure of the steel [51–53]. Thus, as a result of the refinement of the microstructure, an improvement in the impact toughness is expected.

As it has been mentioned, most of the studies conducted have been focused on the use of RE in wrought steels and there is limited reliable and detailed information in the literature to understand the influence of RE additions on the toughness of cast peritectic steels, from which the toughness of deformed steels can be also inherited. In the other words, what occur during the solidification process and the interaction between the inclusions and matrix, in such peritectic steels (in the presence of RE), have not been the subject of the reported studies, even working on the cast grades. Aimed at clarifying these issues, in this study, about 200 ppm of RE (Ce + La) has been added to a low carbon microalloyed steel. Microstructural examinations and deep fractography of the fracture surfaces, in the cast condition, allowed us to understand the contributions of RE to the impact toughness of the studied steel.

2 Experimental Procedures

2.1 Materials

A clean scrap steel was melted in a 100 kg capacity induction furnace under an open air atmosphere. After complete melting, alloying elements as well as carbon content were adjusted and then the melt was deoxidized by aluminum in order to obtain the base microalloyed steel. Chemical composition of the steel was measured by using Optical Emission Spectrometry (OES: ARL 3460) technique onsite. The composition of the base steel is given in Table 1.

A total of 7 g of a Misch metal (37.8 wt% La and 62.1 wt% Ce) was placed at the bottom of a 25 kg capacity carrying ladle. Then, half of the melt was poured into the ladle to ensure obtaining the same composition as the base steel but with the RE addition. The last step of casting was taken by pouring two melts into preheated sand molds with Y-block shape cavities inside. The amount of RE in the investigated steels was measured by Inductively Coupled Plasma (ICP: OPTIMA 7300 DV) technique; the results are shown in Table 2. This table also gives the amount of O and N in the ingots measured by means of a gas analyzing equipment, model: LECO TC-436 AR.

Table 2 Amounts of rare earth elements (La and Ce), O and N in the studied samples

Steels	Elements, in ppm				
	Ce	La	Ce + La	O	N
Base	< 10	< 10	–	96 ± 10	113 ± 4
RE-added	127.0	72.5	199.5	93 ± 6	112 ± 3

Table 3 The maximum temperature at which the phases present in the base steel according to ThermoCalc predictions

Phase	Temperature (°C)
Al_2O_3	> 1500
MnS	1464
NbC	1177
VC	837

The equilibrium phase diagram (Fe–C) was simulated using ThermoCalc software (TCFE8 database) and the chemical composition of the base steel. According to Thermocalc phase predictions, the solidification of the studied steel starts at about 1516 °C where δ-ferrite nucleates from the melt followed by a peritectic transformation. The solidification process of this steel is complete (solidus temperature) at about 1463 °C where austenite is transformed directly from the remaining melt (below the peritectic temperature). The data regarded with the formation/dissolution temperature of some phases present in the studied steels, extracted from ThermoCalc program, are given in Table 3.

Although the microstructure of the as-cast steels is so coarse and they are usually processed by heat treatment to achieve the final desired properties, the microstructure of the as-cast samples were inspected using an Optical Microscopy (OM: NIKON ECLIPSE LV150N) to monitor any influences of RE on the as-cast condition. The rest of the samples were subjected to homogenizing (1100 °C for 5 h) and subsequent normalizing (950 °C for 30 min) treatments in a muffle furnace (model: AZAR M11L) under the air atmosphere.

2.2 Metallographic Sample Preparation and Microstructural Characterization

Samples extracted from the as-cast and normalized heats were prepared using standard metallographic techniques. The samples were mounted in bakelite, dryly ground and then polished with diamond paste of 3 and 1 μm. Especial

cares were taken during the grinding and polishing; controlled force was exerted on the samples during grinding to prevent removal of particles (inclusions) from the surface. Besides, polishing was done using a lubricant (a mix of ethanol and DP-Lubricant Blue) to ensure prevention of oxidation or any possible errors committed through microstructural examinations. In the last step of this preparation, ethanol was also used to remove any products coming from the polishing steps.

Inclusion characterization was carried out on the normalized samples in the as-polished condition to achieve better contrast between the inclusions and matrix. This was done by using OM and Scanning Electron Microscopy (SEM, Hitachi S 4800 J). Imaging in the SEM was carried out using Secondary (SE) and Back Scattered-Electron (BSE) detectors. The SEM was equipped with an Energy Dispersive X-Ray Spectrometer (EDS, Oxford INCA) for the microanalysis of the inclusions/precipitates. An image analysis software (ImageJ 1.47v) was used to measure the roundness factor (R), average area fraction and average area (A) of the inclusions on at least 5 OM micrographs at a same magnification. Assuming the inclusions as circular particles in 2-D, the average equivalent diameter of the inclusions (d) was calculated according to the equation $d = 2\sqrt{A/\pi}$.

The polished as-cast and normalized samples were etched with Nital-2% to reveal the phases present in their microstructure. The etched microstructures of the normalized steels were further inspected under the SEM (Hitachi S 4800 J).

Grain boundaries of ferrite and pearlite were precisely delineated on the OM micrographs by GIMP software (version 2.8). The same image analysis program as utilized for inclusion characterization was employed on these images to measure the volume fraction of pearlite as well as the size of the ferrite grains and pearlite nodules in the studied steels. The same assumption as made for measuring the inclusion size from their average area was made for measuring the size of the ferrite grains and pearlite nodules.

The thickness of GBC in the microstructure of the studied steels was measured from the SEM images. Since the thickness of these carbides is not uniform throughout the microstructure, it is tried to report a thickness size range. The reported data has been obtained from at least 10 observations for each sample.

2.3 Impact test and Fractography

Impact tests were performed at least three times at room temperature using a WOLPERT testing machine (model: AMSLER D-6700) on notched normalized samples, prepared according to ASTM: E23 and the average was reported.

A SEM (model: QUANTA 450) with EDS capability (model: Xflash 6L10) was conducted on the fracture surfaces of the impact samples for inspection of the fracture surfaces as well as microanalysis of the particles appeared on these surfaces. This SEM and its EDS unit were also used for some microstructural observations, like the characterization of GBC.

3 Results

3.1 Inclusion Characterization in the As-Cast Condition

Figure 1 shows OM images of characteristic inclusions in two steels investigated. Observations approve the presence of large inclusions in the base steel with irregular shapes (Fig. 1a). The inspection of these inclusions suggests that the addition of RE to the cast steel leads to a decrease in the size and change their shape to a more spherical geometry (Fig. 1b). A summary of the microstructural characterization undertaken using OM images is given in Table 4 for both steels. It can be realized from this table that RE addition causes a decrease in the average area fraction and average size of the inclusions and also an increase in the roundness factor of the inclusions in the cast steels.

Figure 2 illustrates SEM micrographs along with the microanalyses of a characteristic inclusion found in the base steel. It can be realized that inclusions in the base steel are MnS-Al_2O_3 type. A dark area can be distinguished in the SEM images (Fig. 2a, b) which has been reported as a gap/solid discontinuity caused by different thermal contraction of MnS and the matrix during cooling [54, 55]. However, the removed part of the inclusions might be also generated through the polishing stage. It can be found out from Fig. 2b and the results of spectrum 4 (Fig. 2c) that Nb-rich phase accumulates around MnS consuming the dissolved Nb in the microalloyed steel. This phenomenon has been reported previously in recent study of the authors [50], in which Nb-rich phases (likely as NbC/NbCN) have been observed to form preferentially around MnS particles in the absence of RE elements in the composition. This issue is explained in more detail in Sect. 4.1. Considering the microanalyses of the inclusions, It should be mentioned that if better and accurate limits of detection are searched for the light elements (C, O, N), the use of Wavelength Dispersive Spectroscopy (WDS) would be suggested, thus, the EDS results obtained for the light elements should be taken with caution.

Figure 3 shows SEM micrographs depicting a complex characteristic inclusion observed in the RE-added steel. This inclusion contains a cluster of (RE,Al)-oxide and (RE,Mn)S particles wrapped in a (RE)S matrix. Similarly to the OM observations and compared to the base steel, these SEM

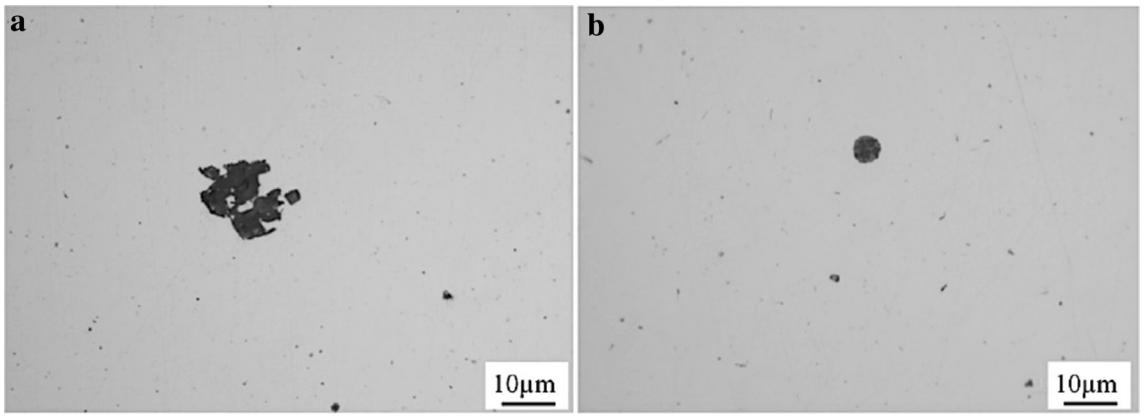

Fig. 1 Inclusions and their morphologies in the **a** base and **b** RE-added steels

Table 4 Inclusion characteristics in the base and RE-added steels

Steels	Area fraction [%]	Average area (A) [μm^2]	Average size (d) [μm]	Roundness factor (R)
Base	0.123 ± 0.004	1.35 ± 0.06	1.31	0.71 ± 0.02
RE-added	0.105 ± 0.004	1.21 ± 0.04	1.24	0.83 ± 0.02

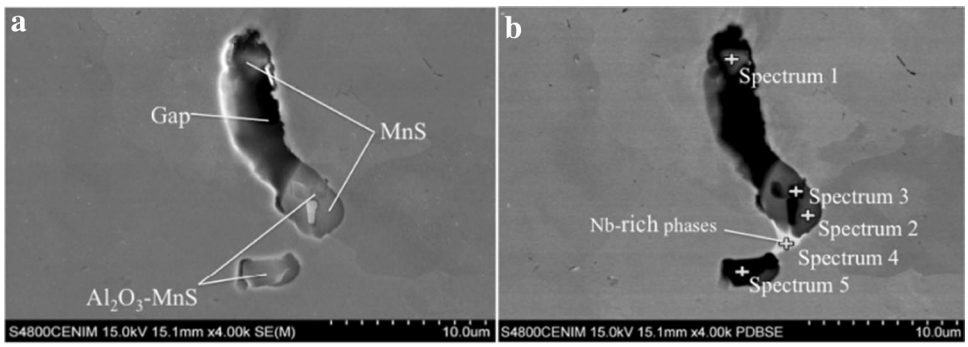

Fig. 2 SEM micrographs in **a** SE and **b** BSE modes and **c** microanalyses of the inclusions observed in the base steel

c

Spectrum	Chemical composition, Wt. %						
	O	C	Al	S	Mn	Fe	Nb
1	8.26	2.99	0.35	19.34	33.80	2.78	-
2	-	2.96	0.63	21.89	34.96	2.30	-
3	16.31	-	12.78	10.02	14.96	2.59	-
4	1.47	9.62	-	-	-	2.19	55.34
5	26.44	-	20.99	4.54	9.57	2.64	-

images show that inclusions in the RE-added steel have a more spherical shape. As expected, the oxide particles appear in the sharp faceted cubic shapes [56]. In addition, it can be deduced from the results of the microanalyses that RE addition of ~ 200 ppm could change the nature of the parent inclusion from MnS-based to RE(S)-based.

3.2 Microstructure of the As-Cast and Normalized Steels

Figure 4 illustrates OM micrographs of the microstructure of the steels in the as-cast condition. The images shown in Fig. 4a, b correspond to the base and RE-added steels, respectively. Both images show a mixture of ferrite and pearlite; however, the distribution of these two phases is not uniform and the microstructures seem to contain coarse and fine grain areas (bimodal microstructure). In addition, from the comparison of both images, it can be concluded that the microstructure of the RE-added steel is finer than that of the base one.

Figure 5 illustrates OM micrographs of the microstructure of the steels investigated in the normalized condition. As for the as-cast microstructures, it seems that the coarse and fine grain areas of ferrite and pearlite (bimodality)

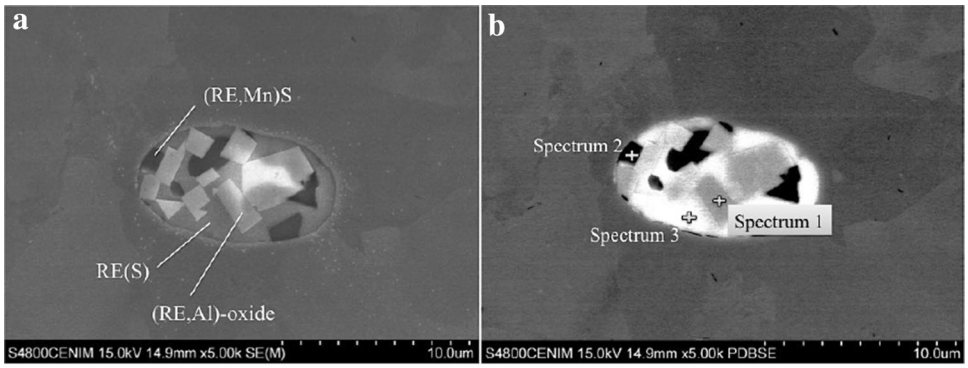

Fig. 3 SEM micrographs in **a** SE and **b** BSE modes and **c** microanalyses of a complex inclusion observed in RE-added steel

c

Spectrum	Chemical composition, Wt. %						
	O	Al	S	Mn	Fe	La	Ce
1	19.71	8.27	-	-	2.09	12.86	37.97
2	2.63	0.65	17.86	28.11	7.44	4.47	13.18
3	1.96	0.71	14.07	-	2.19	13.33	38.08

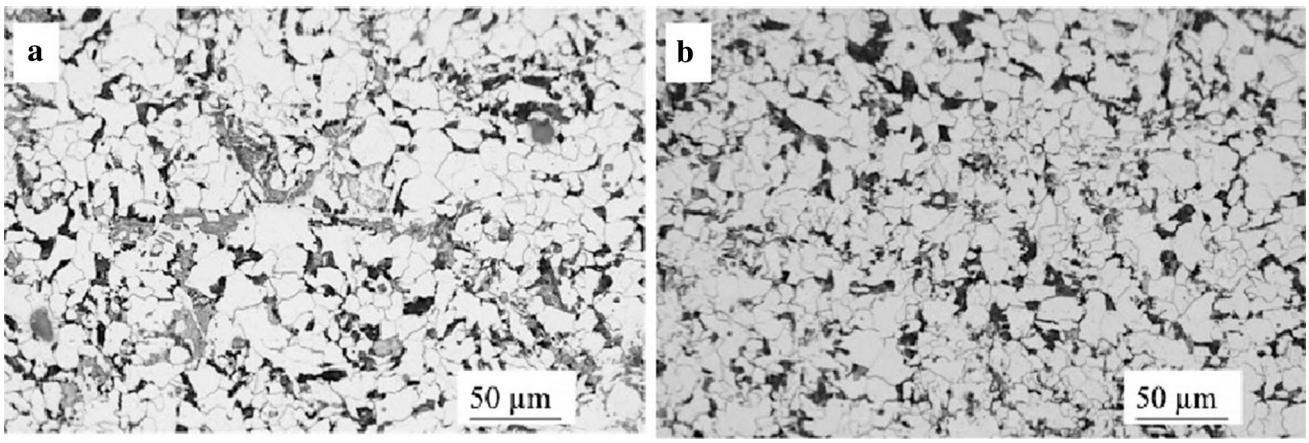

Fig. 4 Microstructure of the as-cast **a** base and **b** RE-added steels

coexist in both steels after applying the normalizing heat treatment. Compared to the base steel (Fig. 5a), it can be observed that the width of the finer grain-sized bands/areas is smaller in the RE-added steel (Fig. 5b). Besides, the overall microstructure in the RE-added steel is finer compared to the base steel, similar to what can be observed in Fig. 4. Ferrite and pearlite are the products of decomposition of the parent phase (austenite); the results suggest that this phase was coarser in the base steel. According to OM observations made on several images similar to those depicted in Fig. 5, the distance between the neighboring large grain regions is about 250–400 µm in the base steel. Although the grain size distribution is more uniform with the RE addition, this separation lies between 200 and 300 µm for the relatively larger grain regions in the RE-added steel. Figure 6 shows SEM images of the normalized samples. It can be seen that compared to the based steel (Fig. 6a), finer and more uniform pearlite nodules can be found in the matrix of RE-added steel (Fig. 6b). However, in these SEM micrographs (at higher magnification) the bimodality is not as obvious as those observed in OM images (Fig. 5).

The pearlite nodule size and its volume fraction have been measured on the several random OM images similar to those shown in Fig. 7; the results are listed in Table 5. It can be deduced from these results that RE addition could decrease pearlite nodule size while it leads to a slight change in the volume fraction of pearlite. In addition, the average ferrite grain size (listed also in Table 5) and the ferrite grain distribution (Fig. 8) of the normalized samples have been measured from the OM images. The average ferrite grain size has been estimated to be 12 and 7 µm for the base and RE-added steels, respectively. Moreover, a clear bimodality can be observed for the base steel (Fig. 8a), while this is not so evident for the normalized RE-added samples (Fig. 8b). One can conclude that, based

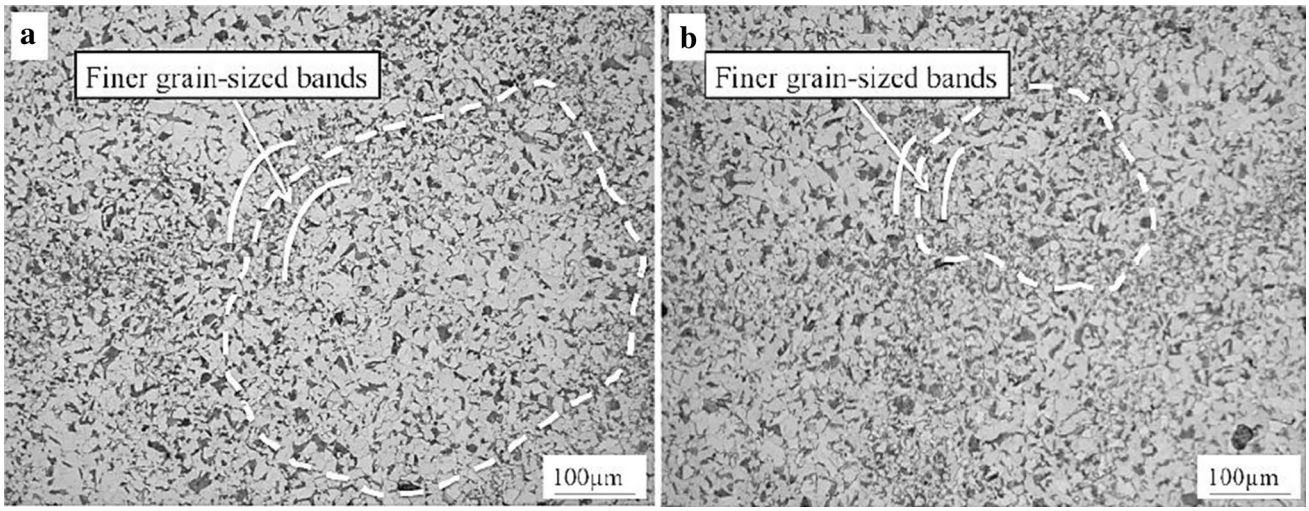

Fig. 5 Microstructure of the normalized **a** base and **b** RE-added steels (lines show the finer grain-sized bands)

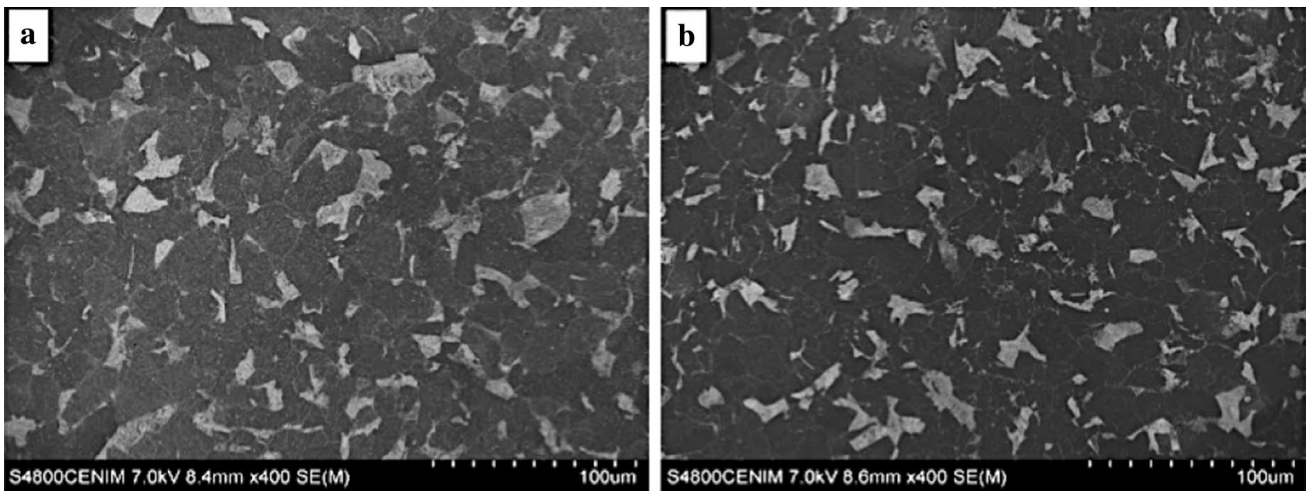

Fig. 6 SEM images showing the microstructure of the normalized **a** base and **b** RE-added steels

on the results shown in Table 5 and Fig. 8, the addition of RE to the base steel helps to refine the microstructure.

3.3 Impact Properties

In introduction section, the influences of the microstructural features on the FATT (as a representative factor of impact property) were discussed. Charpy impact test, as a procedure to measure the amount of energy absorbed by materials during fracture, is performed to determine the toughness of the steel under investigation. The results of this test for the studied steels are given in Table 6. It can be seen that with 200 ppm addition of RE, the steel exhibits a significant increase (about 60%) in impact toughness.

4 Discussion

Previous reports have confirmed that the impact property of ferritic-perritic steels is influenced by the ferrite grain size, volume fraction of pearlite, pearlite nodule size, the presence of grain boundary carbides and the inclusions that exist in these steels [18–20, 23–26, 41]. Besides, it was pointed out that fine precipitates would enhance the impact toughness by affecting the yield stress and inhibiting the dislocation movement, which would retard the fracture. The results obtained in this research indicated that RE could modify the composition and shape of the inclusions in steels and prevent the segregation of the large-sized Nb-rich phases, which might be effective on

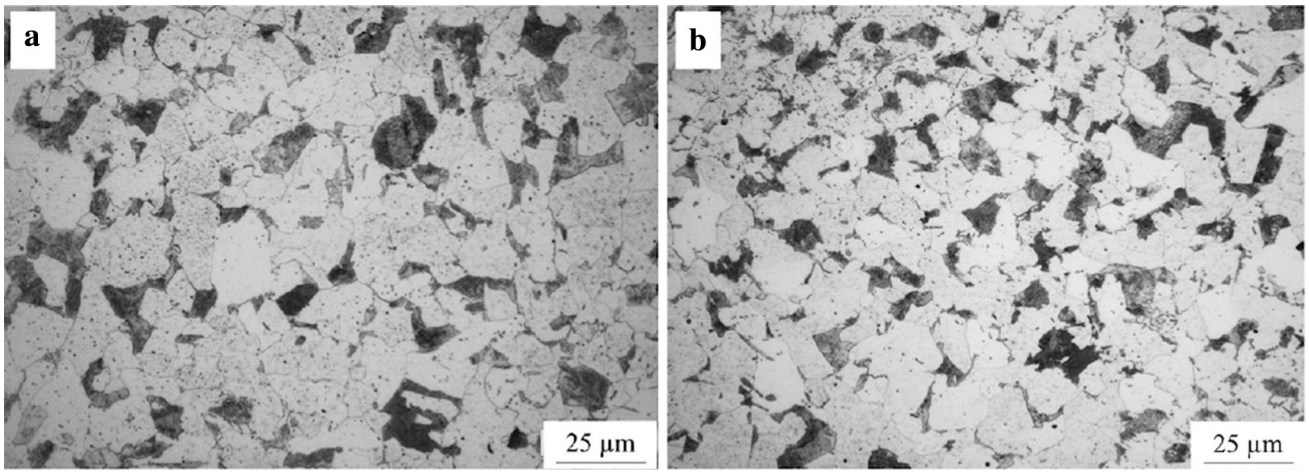

Fig. 7 OM images of the microstructures in normalized condition showing **a** the coarse pearlite nodules in the base and **b** finer pearlite nodules in the finer ferrite matrix in RE-added steel

Table 5 Microstructural characteristics of the normalized steels

Steels	Average of ferrite grain size (µm)	Average of pearlite nodule size (µm)	Volume fraction of pearlite (%)
Base	12 ± 0.6	9 ± 0.4	23 ± 0.8
RE-added	7 ± 0.4	6 ± 0.3	21 ± 0.9

the impact toughness. Moreover, RE addition has led to changes in the features of the phases present in the microstructures (Table 5 and Fig. 8), which may also affect the impact toughness. These issues will be discussed in the upcoming sections.

4.1 The Effects of Inclusion Characteristics on the Impact Properties

Although, in literature, the modification of inclusions by RE in wrought steels has been considered as a main factor improving the toughness property, the results of this study clearly showed that RE addition can affect the inclusion characteristics in the cast condition as well (Table 4 and Figs. 2, 3). In this regard, according to the microanalyses of the inclusions it was found that the RE addition changes the nature of inclusions from MnS-based to (RE)S-based.

It has been shown in Table 4 that the inclusions in the RE-added steel are more spherical which may be attributed to the formation of RE-based particles in the molten steel and their tendency to reach the minimum energy with the melt [57]. According to the data extracted from ThermoCalc software (Table 3), MnS particles form in the pasty region. It is possible for MnS to nucleate on the preexisting inclusions in the melt e.g. on Al_2O_3 or on the RE inclusions. This heterogeneous nucleation would alter the formation temperature of MnS to higher temperatures [27]. Thus, in the last step of solidification, the solidifying grains might impede the dimension and growth of MnS, lowering the roundness factor of this particle. It is generally accepted that the particles with the aspect ratio closer to 1 favor the impact properties

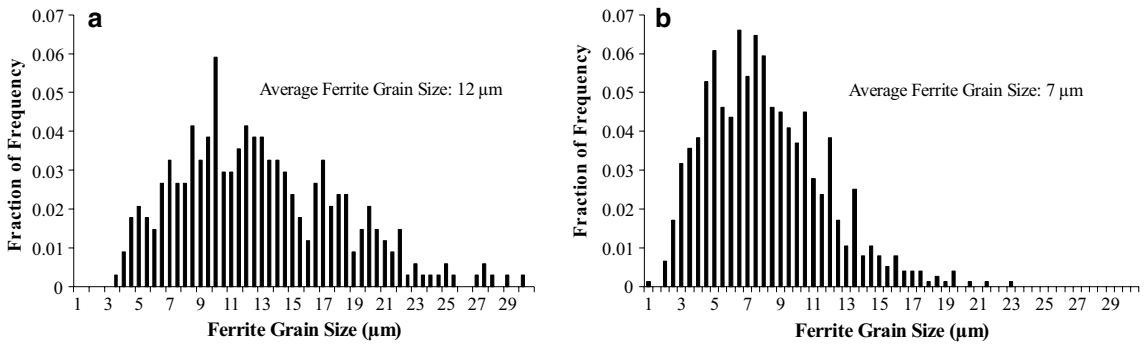

Fig. 8 Size distribution of ferrite grains in the **a** base and **b** RE-added steels (normalized microstructures)

Table 6 The results of the impact test for the investigated steels

Steels	Base	RE-added
Impact energy (J)	63 ± 2	100 ± 3

while sharp (Al_2O_3) or elongated/strip-like particles (MnS) can provide stress concentration and therefore crack initiation centers [48].

The difference in the coefficient of thermal expansion that exists between the matrix and the inclusions leads to the emergence of stress fields or structural discontinuities during the solidification and cooling. The thermal expansion coefficient of MnS is higher than that of steel matrix and, thus, a solid discontinuity/gap may appear at the matrix/MnS interphase during cooling [54]. This gap is expected to have a negative influence on the impact toughness of the steel. In contrast, it has been reported that RE-based inclusions and the steel matrix have similar thermal expansion coefficients [38], therefore, stress concentrations will not be developed during the solidification. Consequently, the gaps between the inclusions and the matrix in the base steel, as the one shown in Fig. 2, could be an additional reason for the brittleness of this steel.

The fracture surfaces of the samples after the impact tests were inspected to clarify the fracture mechanism (Fig. 9). It should be mentioned that no MnS particles have been observed in the fracture surfaces, which could be due to the presence of the debonded areas around these particles. In contrast, the round RE particles could be found in the fracture surface of the RE-added steel, which seem to remain supportive to the matrix even after imposing the impact stresses. It can be deduced from the deformed areas and tiny dimples around the RE-inclusion shown in Fig. 9, likely RE(S) or (RE,Mn)S type, that the presence of these particles would not cause stress concentration and the prospect of crack initiation at these sites would be decreased. The same idea was reported by Sohaciu et al. [54] where it is claimed that the rate of crack propagation is influenced by the nature of the inclusion; supportive hard inclusions would decrease the velocity of the crack propagation.

Figure 10 depicts another type of inclusion observed in the fracture surface of the RE-added steel along with its microanalysis. The results of the microanalysis carried out on the shield show that the particle is a RE-base component. The SEM image reveals some particles similar to the particles/cluster shown in Fig. 3. As it can be seen, the shield of the complex inclusion (a matrix of RE(S)) has been broken due to the impact stresses. The faceted particles inside are visible which according to the microanalyses shown in Figs. 3 and 10, seems to be a (RE,Al)-oxide cluster. It is noteworthy that the content of oxygen and aluminum given in Fig. 10c might refer to the cluster adjacent to the analyzed area due to the excitation volume (in 3D) in X-Ray spectroscopy. In fact, the enclosure of the RE component has acted as a shield and prevented the contact between the sharp cubic oxide particles and the matrix which, in turn, has probably contributed to the enhancement of the impact toughness of RE-added steel (Table 6).

Apart from shape and composition of the inclusions, according to Fig. 2, it was found that coarse Nb precipitates form around MnS particles. The formation of these

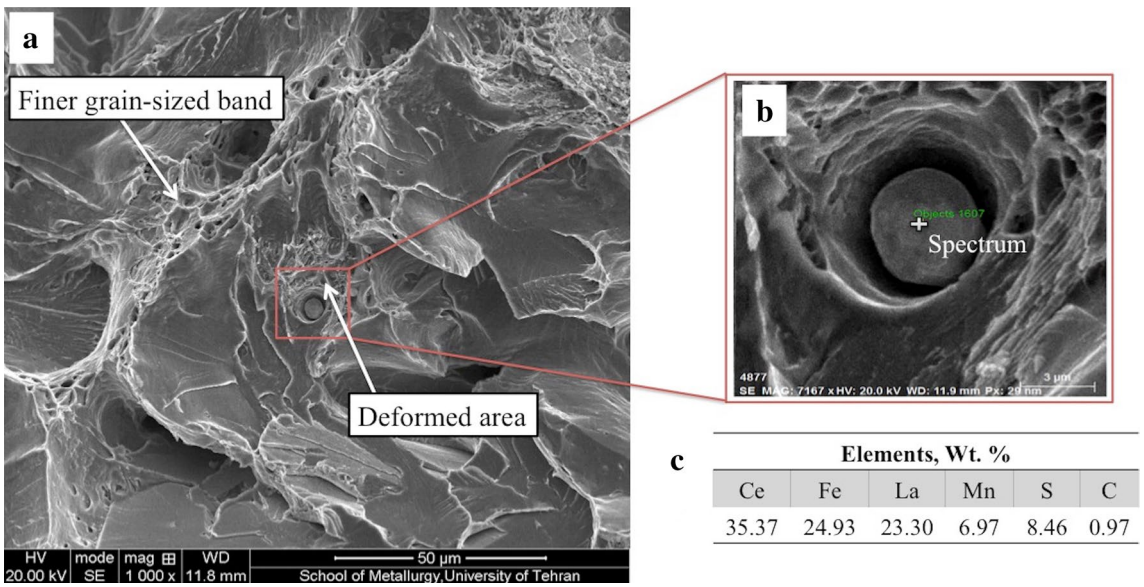

Fig. 9 **a** SEM and **b** magnified SEM micrographs of the fracture surface of the RE-added steel showing deformed areas around RE-based particle and **c** EDS results of the selected point (spectrum) on the inclusion

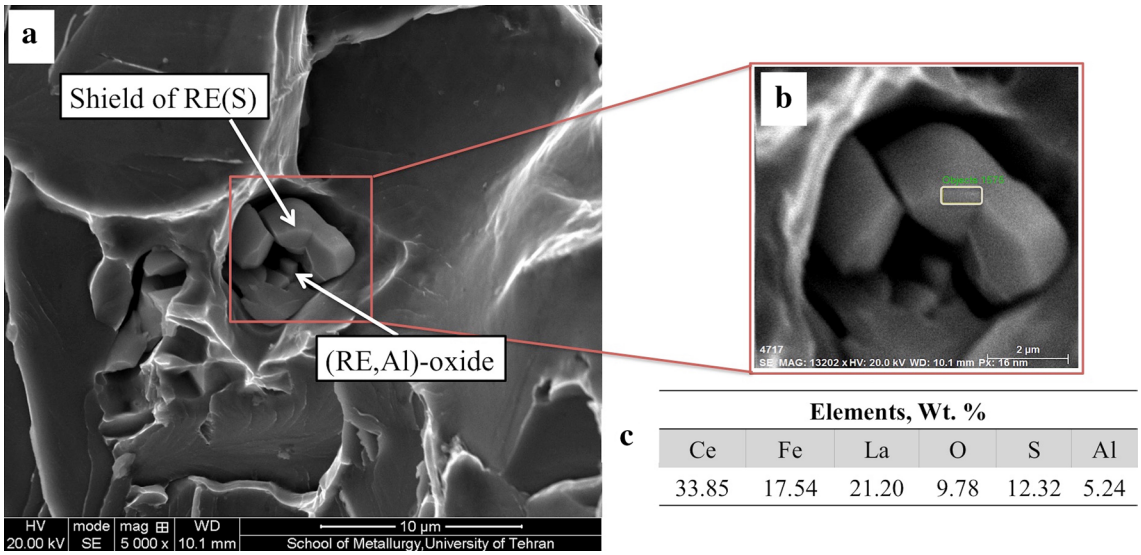

Elements, Wt. %					
Ce	Fe	La	O	S	Al
33.85	17.54	21.20	9.78	12.32	5.24

Fig. 10 **a** SEM and **b** magnified SEM micrographs showing a complex inclusion on the fracture surface of RE-added steel and **c** EDS results of the selected area on the shield of the inclusion

precipitates would reduce the amount of Nb in solid solution necessary for nanoprecipitation. It should be mentioned that annealing temperatures higher than ~ 1200 °C would be required to dissolve these Nb-rich precipitates (Table 3) in order to reprecipitate them in the matrix. This issue has been reported recently by the authors in this type of steels [50] where it was observed that the segregation of the large Nb-rich phases takes place only on MnS and RE addition could suppress the formation of MnS and these segregated areas. As it is proposed there, this phenomenon is related to the higher thermal expansion coefficients of MnS compared to the steel matrix (delta ferrite) during the solidification process, which could take place in such low carbon/peritectic steels. Subsequent stress fields and debonded areas at the interface of MnS and matrix are able to stimulate the formation of large Nb-rich phases (with high formation temperature) around this particle. It should be mentioned that due to removal of these phases (MnS and Nb-rich phases) during the sample preparation, their characterization by TEM was very difficult. However, they have been deeply studied under the SEM. Although the quantitative results obtained by microanalysis (in SEM) for the light elements like C and N are not reliable, qualitative comparisons demonstrated that, compared to the matrix, the Nb-rich phases accommodate more carbon, proposing that these areas can be considered as Nb-carbides/carbonitrides (Fig. 2). Thus, it can be anticipated that the accumulation of large Nb-rich phases around MnS (in the base steel) would lower the amount/efficiency of solute Nb necessary for Nb-nanoprecipitation. In steels with 200 ppm of RE, the formation of MnS has been inhibited (because of previous formation of RE-sulfide/oxysulphide), thereby, Nb atoms would be uniformly distributed as solid solution, promoting Nb-precipitation during cooling. Accordingly, some Nb-nanoprecipitates have already been distributed in the matrix of the RE-added steel even in the cast condition. Hereupon, the higher population density of the nanoprecipitates present in the RE-added steel would contribute to the enhancement of impact toughness.

4.2 Contribution of the Matrix Grain Size Distribution to the Impact Properties

After casting, the optical micrographs shown in Fig. 4 illustrate bimodal ferrite-pearlite microstructures with coarse and fine regions in the both investigated steels. Besides, although the ferrite and pearlite nodule size was not measured in the as-cast condition, it is clear that the microstructure of the RE-added steel is finer compared to the based steel. It is well known that crack propagation and, consequently, the impact toughness are greatly affected by the grain size. Unveiling why the addition of RE-elements may affect the parent austenite microstructure of microalloyed steels that originated these ferritic-pearlitic microstructures is, thus, of key importance.

The appearance of bimodality in the microstructure of microalloyed steels can be created during the different production steps such as solidification, reheating (where pinning effects of precipitates and abnormal grain growth would have a contribution to it), and hot deformation i.e. rolling processes [58, 59]. Considering the fact that the steels studied in this work have not experienced any deformation processes, the contribution of the latter item should be ignored. Besides, since the Nb nanoprecipitation has not been optimized by thermomechanical processing treatments,

the role of these precipitates on the austenite grain size can be assumed to be insignificant at high temperatures. In this regard, Davis et al. [60] claimed that having an inhomogeneous distribution of the precipitates is not sufficient itself to promote a duplex/bimodal grain size microstructure and there should be an additional reason for such observations. Although the studied steels have passed the homogenization and normalizing treatments where Zener effect of the precipitates could have an influence on pinning of the boundaries, such bimodality existed in the as-cast (solidified) structure as well, where the samples are not reheated to high temperatures. This somehow implies that the bimodality observed in the heat treated samples conceivably arises from the solidification stage; it has been shown that normalizing heat treatment applied after casting has not been able to homogenize the grain size as a bimodal microstructure with finer grain size can be observed in RE-added steel (Fig. 5). Hence, the effect of RE addition on the grain size and its distribution could be considered from the following point of view.

Non-metallic inclusions such as oxides appear in various stages of the solidification of steels. These may act as the cores for the heterogeneous nucleation to refine solidification structure as well as to inhibit grain growth by Zener pinning in the solid state [28, 32, 35–37]. The heterogeneous nucleation takes place when two main conditions are met during the solidification [61]:

I. The lattice misfit between the particle and the solidifying phase must be less than 6%; when the lattice misfit is small at the melting point of the alloy, a proposed nucleation particle will facilitate the nucleation of other solid. Experimental evidences have shown that the lattice misfit of the RE-based particles with the steel matrix is less than 6% [32, 36, 48, 62] which would reduce the nucleation barrier and promote the solidification of the new solid phase.
II. The melting point of the candidate nuclei must be higher than that of the alloy. Computational calculations support that the melting points of RE oxides/sulfides (Table 7) are much higher than the melting point of the investigated steels [63] and they form stable compounds right after the introduction of the misch metal to the melt [30, 45, 46, 48].

Tuttle [64], in addition to these criteria, also considered the wettability and crystallographic structure of RE-based inclusions in steels which fulfill the requirements to serve as potent heterogonous nucleation sites during solidification.

The structure of low carbon steels, which experience peritectic transformation, is strongly dependent on the number of solidification nucleation sites. It has been reported that the number of nucleation sites for the peritectic austenite to form is low which would usually increase by the presence

Table 7 Melting points of some typical RE inclusions [63]

Compound	Melting point (°C)
Ce_2O_3	~2177
La_2O_3	~2249
Ce_2S_3	~2150
La_2S_3	~2099

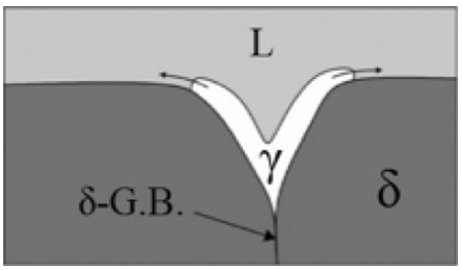

Fig. 11 Schematic of a peritectic reaction (nucleation of γ) on the grain boundary of δ (arrows show the direction of γ growth)

of heterogeneous nucleation sites [12]. Thus, heterogonous nuclei would promote the formation of additional solidified grains to grow in the melt until hard impingement takes place, resulting in a reduction of the δ-ferrite grain size. In addition, it has been reported that the grain boundaries of the δ-ferrite are preferential sites for the peritectic reaction [14, 15]. A schematic of this phenomenon is depicted in Fig. 11. For that reason, when the number of the nucleating agents (RE compounds in the melt) for δ-ferrite formation increases, a higher density of the δ-ferrite grain boundaries are provided for the nucleation of the peritectic austenite. These phenomena will eventually result in the refinement of γ grains at high temperature, also resulting in the refinement of the product microstructure upon cooling to room temperature and, consequently, the enhancement of the impact toughness. Moreover, the finer grains bands observed in the as-cast (Fig. 4) and normalized (Fig. 5) conditions would arise from the structure formed at last step of solidification. At that stage, the temperature of the melt has been probably dropped and possible thermal and/or constitutional undercooling has been provided for the melt remained between the solidifying grains; it is suggested that in last stage of solidification, heat has been removed from the melt by convection in the molten metal or by conduction process through the mold (thermal undercooling) and also concentration of solutes in the remained melt has increased, providing the constitutional undercooling [57]. As a matter of fact, the larger the undercooling the more populous solidification nuclei would be, resulting in refinement of the solidified grains. Both of the aforesaid mechanisms would provide negative Gibbs free energy required for solidification of the remained

melt in the studied steels, creating a finer grains between existed relatively large solidified grains.

In addition to these mechanisms, existence of the fine grain sized bands between the larger grain regions would be possibly related to the different stages of austenite formation during the solidification process. It should be mentioned that, although ThermoCalc software predicts the phase diagram in equilibrium condition, based on the chemical composition of the base steel, the extracted data approved that the studied steel is a hyper-peritectic type. In fact, solidification of this steel starts with deposition of delta ferrite in the melt followed by peritectic transformation. As it was mentioned above, this transformation requires volume diffusion from the melt through the layer of the γ-phase towards the δ-phase direction, which is believed to have a low kinetic rate [15], resulting in coarse austenite grains. In hyper-peritectic steels, the solidification process will not end after completion of the peritectic transformation and liquid still coexists with austenite. The remaining melt would directly transform to austenite at lower temperature resulting in finer austenite grains at last stage of solidification.

The postulated consequence of these scenarios in the as cast as well as in the normalized conditions has been shown in Figs. 4 and 5.

To evaluate the effect of bimodality on the impact toughness, fracture surfaces of the impact samples were further examined for both steels. Figure 12 shows a fractograph of the base steel in which two well different areas can be recognized. Aforementioned areas could be related to the finer grain-sized bands and larger grain regions. The bands shown in this figure include very fine dimples corresponding to a ductile fracture. Microstructural inspections (Fig. 5) showed that the distance between adjacent larger grains area is longer in the base steel and consequently, the fraction of the finer grains in the base steel is lower than that in the RE-added steel. The fracture surface of the RE-added steel illustrated in Fig. 9 proves that this separation is limited to a much shorter distance in RE-added steel. It has been claimed that the presence of coarse grains in front of the ductile crack tip may promote brittle/cleavage fracture, while fine grains resist cleavage initiation and the ductile crack propagates further, resulting in the absorption of higher impact energy [65, 66]. In this regard, Bengochea et al. [67] deduced that in a heterogeneous ferrite microstructure, with the presence of a relatively important number of large grains in the final microstructure, mechanical properties of the steel, mainly the toughness, would be impaired in spite of the small mean grain size. Therefore the higher impact toughness obtained in RE-added steel would be expected.

Higher magnification of the larger grains region in the base (Fig. 13a) and finer grain-sized band in the RE-added (Fig. 13b) steels are shown in SEM images. It is clear that

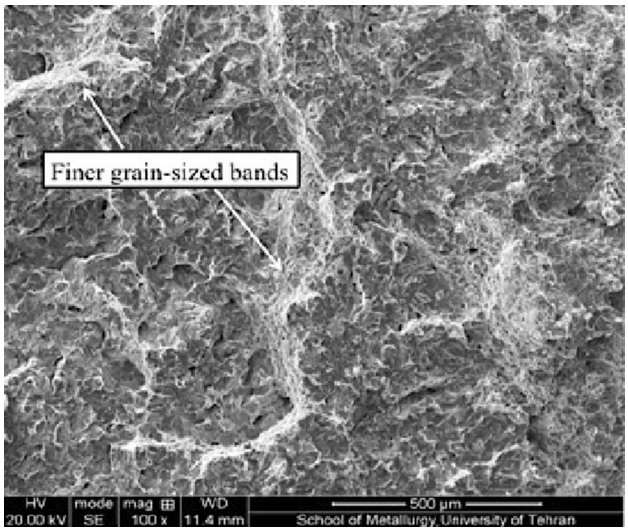

Fig. 12 SEM fractograph showing finer and larger grain regions in the fracture surface of the base steel

these images correspond to the brittle/cleavage (Fig. 13a) and ductile (Fig. 13b) fractures.

To sum up, it could be assumed that the both cleavage and ductile mechanisms for fracture (derived from the large and fine grain areas, respectively) can be found in the base and RE-added steels. While, compared to the base steel, the fraction of the ductile mode (determined by the dimples appeared on the fracture surface) is higher in RE-added steel.

4.3 Contributions of Pearlite and GBC to the Impact Properties

The data extracted from the pearlite phase characterization show that the RE-addition could refine the pearlite nodules and slightly decrease the volume fraction of pearlite (Table 5). It is reported that pearlite volume fraction would affect the impact property; the lower the volume fraction of perlite, the higher is the impact energy [20]. The slight change in the volume fraction of pearlite by the RE-addition could be attributed to the grain refinement achieved by RE addition which was discussed in Sect. 4.2. In this case, Aranda et al. [68] have reported that the finer austenite grains provide more grain boundary areas which will be used as nucleation sites for proeutectoid ferrite, thus, formation of ferrite is promoted and a higher fraction of ferrite (lower fraction of pearlite) in the final microstructure is expected.

In spite of the fact that the change in the pearlite volume fraction caused by RE-addition is insignificant and it may have a minor influence on the impact toughness, the nodule size is effectively affected by RE-addition. This value is controlled by the transformation temperature and prior austenite grain size; the higher the transformation temperature and the

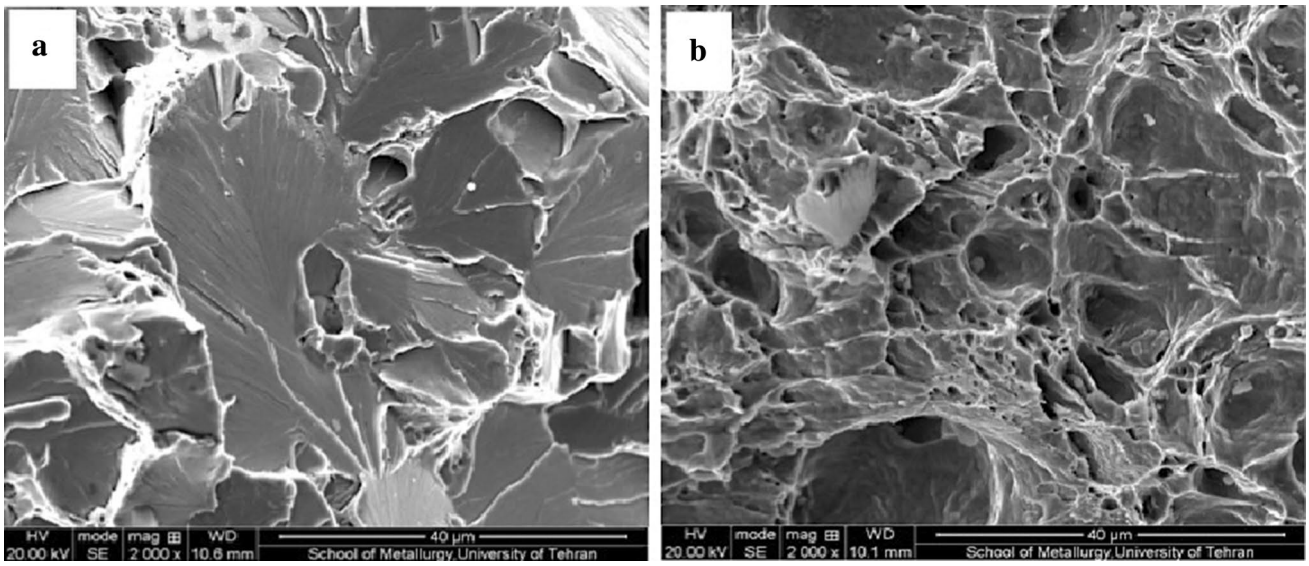

Fig. 13 SEM images showing the fracture surface of **a** larger grains area in the base and **b** finer grain sized band in RE-added steels

coarser the prior austenite grain size, the larger is the nodule size [21]. The experimental results described in Table 5 show that RE-addition could refine the nodule size. Since the history of the base and RE-added steels is the same, finer nodule size could be attributed to the finer austenite grains obtained in the RE-added steel. Figure 14 illustrates a relatively large pearlite nodule on the fracture surface of the base steel which can be considered as an origin of the cleavage fracture.

It has also been discussed that an approximately linear relationship exists between the impact transition temperature and the square root of the carbide thickness (t). It is reported that for low carbon steels, this value is influenced by the composition (Mn %), ferrite grain size (D) and cooling rate (T) which can be expressed by the following equation [20, 27]:

$$t = 0.789 - 0.00609D^{-\frac{1}{2}} - 0.267\%\,\mathrm{Mn} - 0.0291T^{\frac{1}{2}} \quad (4)$$

Since the chemical composition (except RE content) and the history of the steels under investigation are the same, thick Grain Boundary Carbides, GBC, (Fig. 15a) can be attributed to the larger grains observed in the base steel. As a well known fact, compared to austenite, ferrite accommodates much lower amount of carbon. Thus, when proeutectoid ferrite grows, the excess carbon redistributes to the adjacent austenite, likely to their boundary.

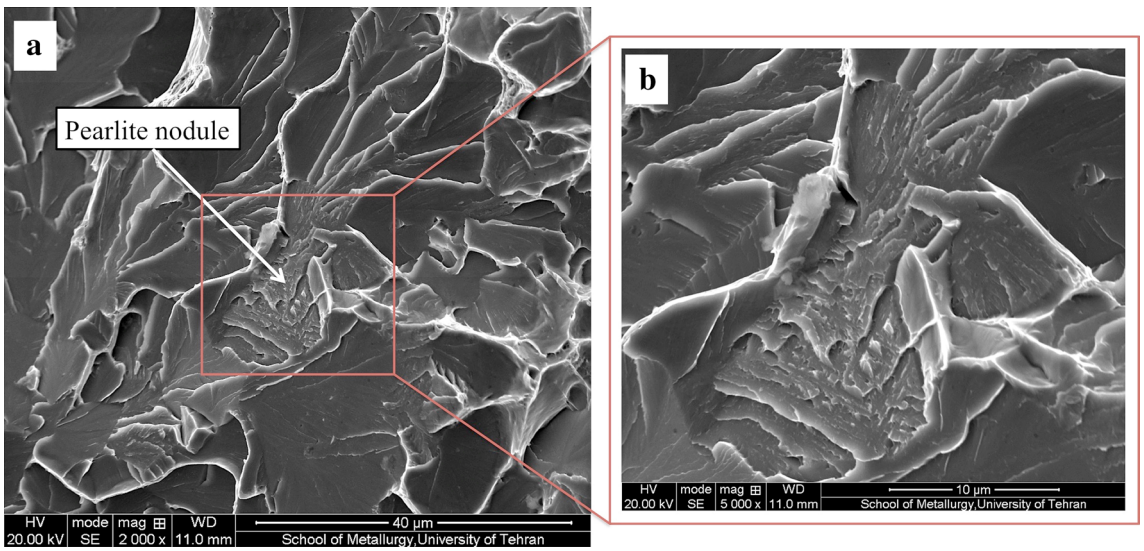

Fig. 14 **a** SEM and **b** magnified SEM fractographs showing a pearlite nodule on the fracture surface of the base steel

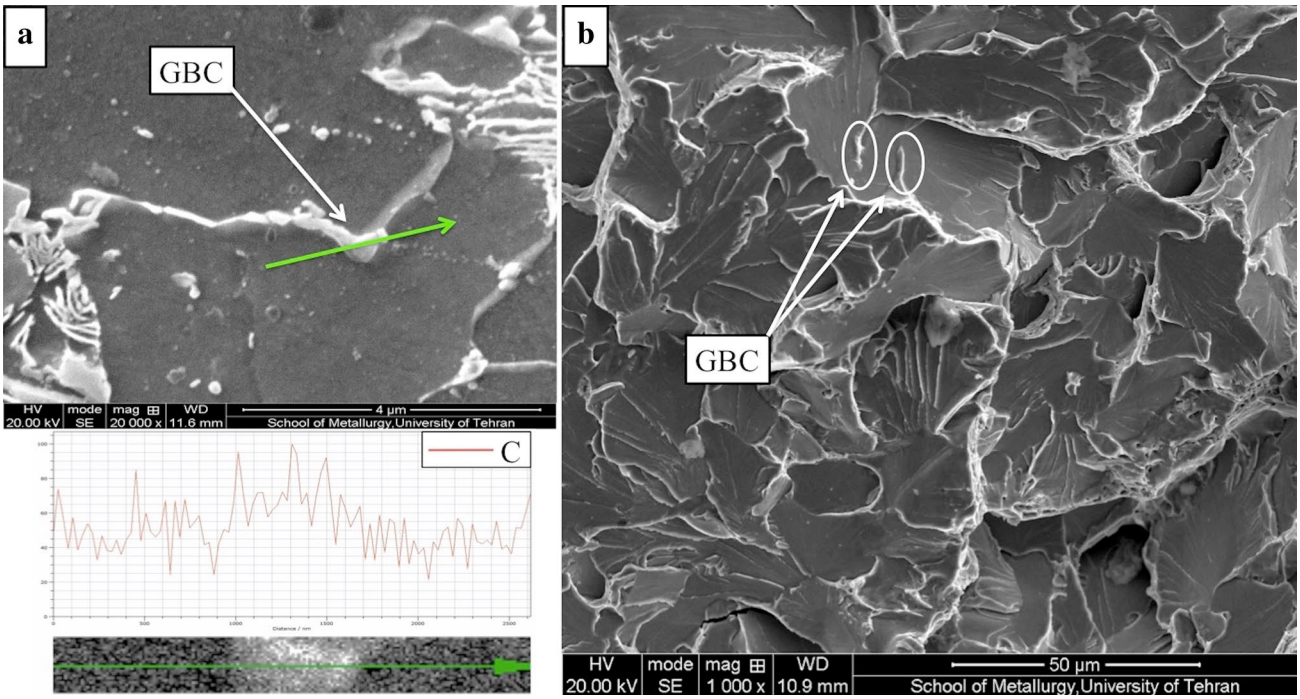

Fig. 15 **a** SEM image along with a line scan microanalysis of the grain boundary precipitate and **b** SEM fractograph showing GBC resulting in cleavage fracture in the normalized base steel

Therefore, in steels with larger ferrite grains (base steel), higher amount of carbon would be pushback to the boundary, resulting in formation of thicker carbide (cementite) formed at this area. The effect of GBCs on the fracture surfaces of this steel is shown in Fig. 15b. The same idea and observations have been reported elsewhere [20, 24, 27] where it is confirmed that the cracking of this type of carbides is an essential feature of the cleavage process, deteriorating the toughness property. The GBCs could be also found in RE-added steel (Fig. 16) while compared to the base steel, their thickness is smaller and their density is lower; the thickness of most of the GBCs observed in the base steel is in the range of 0.05–0.60 µm, while this value for most of the GBCs in RE-added steel is in the range of 0.05–0.30 µm. As it was mentioned above, according to Mintz [20], the thickness reported for the GBCs found in RE-added steel mostly lies in out of the effective thickness range, hence, it does not seem to be as detrimental as GBCs observed in the base steel.

Although the results obtained in this study disclosed the influences of RE addition on the impact toughness of the steels under investigation, further researches might be necessary for better understanding the link between the addition of these elements to the composition and the microstructural variations and subsequently to the other mechanical properties of such a low carbon cast Nb-microalloyed steel.

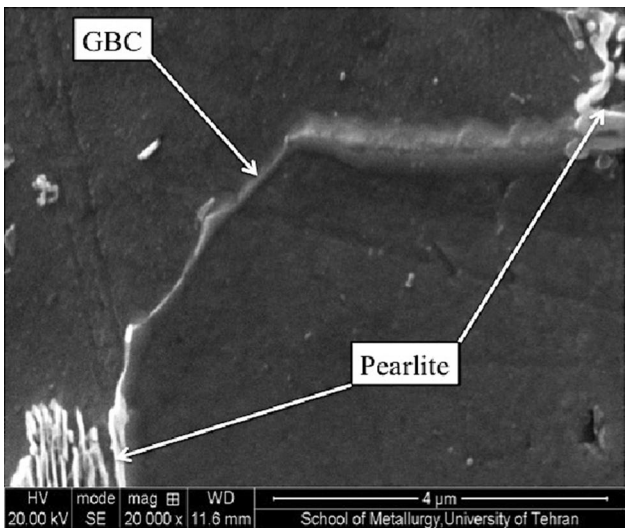

Fig. 16 SEM image showing a relatively thin GBC in the normalized RE-added steel

5 Conclusions

This experimental report provides an improvement in the understanding of the influence of rare earth (RE) elements (La, Ce) on the microstructure and impact toughness of cast ferritic-pearlitic microalloyed steels. It can be

proposed that the modification of the inclusions and their effects on solidification process (including the peritectic transformation) would have a great contribution to the impact toughness of the cast steel. The main outcomes of this work can be summarized as follows:

1. The combined RE addition of La and Ce at the rate of 200 ppm affected the inclusion characteristics and changed their nature from MnS-based to RE(S)-based. Inclusions appeared in the RE-added steel were found to be smaller and more spherical, with a lower average area fraction. All these factors contribute positively to enhancing the impact toughness of the RE-added steel compared to the base one.
2. MnS particles were found to serve as preferential nucleation sites for large Nb-rich phases (likely as NbC/NbCN), formation of which could be suppressed by RE addition. Consequently, it can be anticipated that more solute Nb are possibly available for the formation of nanoprecipitates in RE-added steel, which is believed to have a contribution to the enhancement of impact energy absorbed.
3. In the normalized condition, finer microstructural components (finer pearlite nodules in the finer ferrite matrix) and a slight reduction in pearlite volume fraction were obtained by RE-addition, where the bimodality was redressed as well. The finer grain-sized bands, whose volume fraction was higher in the RE-added steel, are linked to the very tiny dimples on the fracture surfaces and contribute to the improvement of impact toughness.
4. The results of SEM observations showed that the relatively thick GBC caused by the large ferrite grains existed in the microstructure of the base steel, which would impair the impact toughness.
5. The microstructural characterization and the fractography analyses allowed us to conclude that the aforesaid microstructural variations observed in the RE-added steel were the main reasons to explain the notable enhancement of the impact toughness (about 60%) in the microalloyed steel investigated.

Acknowledgements The authors from University of Tehran gratefully acknowledge the financial support provided by the office of international affairs and the office for research affairs, college of engineering, for the Project Number 8107009.6.34. The authors from CENIM-CSIC would like to acknowledge the financial support from Comunidad de Madrid through DIMMAT-CM_S2013/MIT-2775 Project. Authors are grateful to the Phase Transformations and Microscopy labs from CENIM-CSIC. Mr. Javier Vara Miñambres from the Phase Transformations lab (CENIM-CSIC) is gratefully acknowledged for his continuous experimental support.

References

1. J. Rassizadehghani, H. Najafi, M. Emamy, G. Eslami-Saeen, J. Mater. Sci. Technol. **23**, 779 (2007)
2. J.R. Davis, *Alloying: Understanding the Basics* (ASM International, Russell Township, 2001)
3. H. Najafi, J. Rassizadehghani, S. Norouzi, Mater. Des. **32**, 656 (2011)
4. K.Y. Xie, T. Zheng, J.M. Cairney, H. Kaul, J.G. Williams, F.J. Barbaro, C.R. Killmore, S.P. Ringer, Scr. Mater. **66**, 710 (2012)
5. H. Najafi, J. Rassizadehghani, S. Asgari, Mater. Sci. Eng. A **486**, 1 (2008)
6. B. Korojy, H. Nassar, H. Fredriksson, Ironmak. Steelmak. **37**, 63 (2010)
7. M.H. Trejo, E.A. Lopez, J.J. Ruiz, M.D. Mondragon, J. Castro Roman, H.S. Tovar, Met. Mater. Int. **16**, 731 (2010)
8. K. Matsuura, M. Kudoh, Met. Mater. Int. **4**, 562 (1998)
9. D.H.S. John, L.M. Hogan, Acta Metall. **25**, 77 (1977)
10. S. Akamatsu, M. Plapp, Curr. Opin. Solid State Mater. Sci. **20**, 46 (2016)
11. H. Nassar, *On Peritectic Reactions and Transformations and Hot Forming of Cast Structures*. Doctoral PhD dissertation, Department of Material Science and Engineering, School of Industrial Engineering and Management Royal Institute of Technology (KTH), Stockholm, Sweden (2009)
12. I.M.E. Kalinushkin, Yu. Taran, L. Tykhonuk, Metalurgija **41**(3), 131 (2002)
13. D. Stefanescu, *Science and Engineering of Casting Solidification*, 2nd edn. (Springer, Berlin, 2009)
14. S. Griesser, M. Reid, C. Bernhard, R. Dippenaar, Acta Mater. **67**, 335 (2014)
15. H. Shibata, Y. Arai, M. Suzuki, T. Emi, Metall. Mater. Trans. B **31**, 981 (2000)
16. M. Kudoh, K. Igarashi, K. Matsuura, K. Ohsasa, SIJ Int. **48**, 334 (2008)
17. T. Lipiński, A. Wach, Arch. Foundry Eng. **14**, 55 (2014)
18. A.J. DeArdo, SIJ Int. **35**, 946 (1995)
19. A.M. Elwazri, P. Wanjara, S. Yue, Mater. Sci. Eng., A **404**, 91 (2005)
20. B. Mintz, W.B. Morrison, A. Jones, Metals Technol. **6**, 252 (1979)
21. B. Garbarz, F.B. Pickering, Mater. Sci. Technol. **4**, 328 (1988)
22. F.P.L. Kavishe, T.J. Baker, Mater. Sci. Technol. **2**, 816 (1986)
23. K.K. Ray, D. Mondal, Acta Metall. Mater. **39**, 2201 (1991)
24. M.S. Bingley, Mater. Sci. Technol. **17**, 700 (2001)
25. S. Shanmugam, R.D.K. Misra, T. Mannering, D. Panda, S.G. Jansto, Mater. Sci. Eng. A **437**, 436 (2006)
26. I. Gutierrez, Rev. Metal Madr. **50**, 1 (2014)
27. I. Gutiérrez, Mater. Sci. Eng. A **571**, 57 (2013)
28. M. Wintz, M. Bobadilla, J. Lehmann, H. Gaye, SIJ Int. **35**, 715 (1995)
29. Y. Nuri, T. Ohashi, T. Hiromoto, O. Kitamura, Trans. Iron Steel. Inst. Jpn. **22**, 399 (1982)
30. J. Yang, D.-N. Zou, X.-M. Li, Z.-Z. Du, J. Iron Steel Res. Int. **14**, 47 (2007)
31. L. Wang, Q. Lin, J. Ji, D. Lan, J. Alloys Compd. **408–412**, 384 (2006)
32. L.M. Wang, Q. Lin, L.J. Yue, L. Liu, F. Guo, F.M. Wang, J. Alloys Compd. **451**, 534 (2008)
33. S.K. Paul, A.K. Chakrabarty, S. Basu, Metall. Trans. B **13**, 185 (1982)
34. A. Grajcar, M. Kaminska, U. Galisz, L. Bulkowski, M. Opiela, P. Skrzypczyk, JAMME **55**, 245 (2012)
35. S. Morioka, H. Suito, SIJ Int. **48**, 286 (2008)

36. H. Suito, H. Ohta, S. Morioka, SIJ Int. **46**, 840 (2006)
37. G.M.A.S. Hideaki, SIJ Int **39**, 1289 (1999)
38. F. Pan, J. Zhang, H.L. Chen, Y.H. Su, C.L. Kou, Y.H. Su, S.H. Chen, K.J. Lin, P.H. Hsieh, W.S. Hwang, Materials **9**, 417 (2016)
39. K. Chang, W. Feng, L.-Q. Chen, Acta Mater. **57**, 5229 (2009)
40. A.P. Gulyayev, Y.A. Ul'yanin, Met. Sci. Heat Treat. **3**, 460 (1961)
41. A.F. Belyakova, Y.V. Kryankovskii, I.V. Paisov, Met. Sci. Heat Treat. **7**, 588 (1965)
42. K.J. Handerhan, W.M. Garrison, Scr. Metall. **22**, 409 (1988)
43. M.W. Garrison Jr., L.J. Maloney, Mater. Sci. Eng. A **403**, 299 (2005)
44. H.L. Liu, C.J. Liu, M.F. Jiang, Mater. Des. **33**, 306 (2012)
45. J. Gao, P. Fu, H. Liu, D. Li, Metals **5**, 383 (2015)
46. X. Liu, J.-C. Yang, L. Yang, X.-Z. Gao, J. Iron Steel Res. Int. **17**, 59 (2010)
47. X. Chen, Y. Li, Mater. Sci. Eng. A **444**, 298 (2007)
48. J. Lan, J. He, W. Ding, Q. Wang, Y. Zhu, SIJ Int. **40**, 1275 (2000)
49. H.L. Liu, C.J. Liu, M.F. Jiang, Adv. Mater. Res. **129–131**, 542 (2010)
50. H. Torkamani, S. Raygan, C. Garcia Mateo, J. Rassizadehghani, J. Vivas, Y. Palizdar, D. San Martin, Metals **7**, 377 (2017)
51. D. San Martin, F.G. Caballero, C. Capdevila, C. Garcia de Andres, Mater. Trans. **45**, 2797 (2004)
52. C. Fossaert, G. Rees, T. Maurickx, H.K.D.H. Bhadeshia, Metall. Mater. Trans. A **26**, 21 (1995)
53. H.R. Wang, W. Wang, J. Mater. Sci. **44**, 591 (2008)
54. M. Sohaciu, C. Predescu, E. Vasile, E. Matei, D. Savastru, A. Berbecaru, Dig. J. Nanomater. Biostruct. **8**, 367 (2013)
55. H. Drar, Mater. Charact. **45**, 211 (2000)
56. A. Muan, E.F. Osborn, *Phase Equilibria Among Oxides in Steelmaking* (Addison-Wesley Pub. Co., Boston, 1965)
57. D.A. Porter, K.E. Easterling, M. Sherif, *Phase Transformations in Metals and Alloys*, 3rd edn. (CRC Press, Boca Raton, 2009)
58. D. Chakrabarti, C.L. Davis, M. Strangwood, Mater. Sci. Forum **500–501**, 613 (2005)
59. D. Chakrabarti, *Development of Bimodal Grain Structures and Their Effect on Toughness in HSLA Steel*, Ph.D. Dissertation, Department of Metallurgy and Materials, School of Engineering, University of Birmingham (2007)
60. C.L. Davis, M. Strangwood, J. Mater. Sci. **37**, 1083 (2002)
61. B.L. Bramfitt, Metall. Trans. **1**, 1987 (1970)
62. Ø. Grong, *Metallurgical Modelling of Welding* (Institute of Materials, London, 1997)
63. M. Opiela, A. Grajcar, Arch. Foundry Eng. **12**, 129 (2012)
64. R. Tuttle, IJMC **6**, 51 (2012)
65. D. Chakrabarti, M. Strangwood, C. Davis, Metall. Mater. Trans. A **40**, 780 (2009)
66. A.S. Kumar, B.R. Kumar, G.L. Datta, V.R. Ranganath, Mater. Sci. Eng. A **527**, 954 (2010)
67. R. Bengochea, B. López, I. Gutierrez, B. López, I. Gutierrez, Metall. Mater. Trans. A **29**, 417 (1998)
68. M.M. Aranda, B. Kim, R. Rementeria, C. Capdevila, C.G. de Andrés, Metall. Mater. Trans. A **45**, 1778 (2014)